

Research Paper

Interactions of Poly(vinylpyrrolidone) with Ibuprofen and Naproxen: Experimental and Modeling Studies

Svetla Bogdanova,^{1,4} Ilza Pajeva,² Petya Nikolova,¹ Ivanka Tsakovska,² and Bernd Müller³

Received September 29, 2004; accepted January 19, 2005

Purpose. To elucidate the differences in the interaction of chiralic ibuprofen (IBP) and naproxen (NAP) with poly(vinylpyrrolidone) (PVP) in a solid state.

Methods. Drugs/PVP physical mixtures and solid dispersions were characterized by scanning electron microscope (SEM), Fourier transform infrared spectrometry (FT-IR), solid state ¹³C NMR spectroscopy, and x-ray diffractometry. Molecular modeling study of the crystal structures and PVP was performed.

Results. A spontaneous conversion of IBP/PVP physical mixtures in a stable glasslike form (solid dispersion) was observed after storage. The enantiomer reacted more strongly than the racemate. NAP did not interact with PVP. The crystal structures of drugs showed differences in the hydrogen bonding, aromatic interactions, molecular energies, and distances inside the crystals. The trimer structure of PVP was built and optimized. It was proposed that each PVP monomer could interact with one IBP dimer in contrast to NAP, where two out of three PVP monomers faced the catemer carboxylic groups.

Conclusions. The differences in the interaction of PVP with racemic IBP, enantiomer IBP, and NAP can be related to the differences in their crystal structures. The correlation between the experimental data and the results of the molecular modeling analysis suggest that the IBP dimer structures are likely to perform HB and aromatic interactions with PVP.

KEY WORDS: ibuprofen, interactions, molecular modeling analysis, naproxen, poly(vinylpyrrolidone).

INTRODUCTION

Recent data (1–4) have shown that 2-(4-isobutylphenyl)propionic acid (ibuprofen) (IBP)/poly(vinylpyrrolidone) (PVP) physical mixtures transform spontaneously into supersaturated solid solutions during storage at ambient conditions and could provoke technological problems with solid dosage form development (4). It is worth noting that the moisture content of the samples is relatively low: 3.8%. Preliminary studies of physical mixtures of other nonsteroidal anti-inflammatory drugs (NSAIDs) from the chemical group of the propionic acid derivatives with PVP revealed a similar phenomenon with 2-(3-benzoylphenyl)propionic acid (ketoprofen) and no interactions and changes in the physical state with 2-(6-methoxynaphth-2-yl)propionic acid (naproxen) (NAP) (4).

This study aims to elucidate the differences observed in the interaction of racemic IBP (rac-IBP), the S-enantiomer of IBP (S-IBP), and the S-enantiomer of NAP (S-NAP) with PVP during mutual cogrinding and coevaporation processes. Fourier transform infrared (FTIR), ¹³C NMR, and X-ray

analysis in solid state of model physical mixtures and their corresponding solid dispersions of varying drug/polymer ratio freshly prepared and after storage were carried out to determine the physicochemical properties of the model preparations. Molecular modeling analysis was applied to explain the suggested influence of the drug crystal arrangement on the drug/PVP interactions.

It was assumed that the crystal packing arrangement and the intermolecular interactions in the crystals set the pattern of the drug/polymer interactions via a competitive hydrogen bonding with the PVP amide group.

MATERIALS AND METHODS

Materials

2-(4-Isobutylphenyl)-propionic acid, Ibuprofen 50 (catalytic process) was purchased from BASF AG (Ludwigshafen, Germany); S-(+)-2-(4-isobutylphenyl)-propionic acid ≥99.0% (ibuprofen) from Fluka Chemie GmbH (Buchs, Switzerland); (S)-(+)-6-methoxy- α -methyl-2-naphthalene acetic acid, 98% (naproxen) from Sigma-Aldrich Chemie GmbH (Steinheim, Germany), and Kollidone K25 from BASF AG (Ludwigshafen, Germany).

Methods

Preparation of Drug/Poly(vinylpyrrolidone) Physical Mixtures and Coevaporates

Physical mixtures were prepared in drug/polymer ratio 1/0.5; 1/1.5, and 1:3 (w/w), respectively, by grinding and mix-

¹ Faculty of Pharmacy, Medical University, Sofia, Bulgaria.

² Centre of Biomedical Engineering, Bulgarian Academy of Sciences, Sofia, Bulgaria.

³ Department of Pharmacy, Christian-Albrecht-University, Kiel, Germany.

⁴ To whom correspondence should be addressed. (e-mail: sbogdanova@pharmfac.acad.bg)

ing with a pestle in a mortar for 10 min and passing through 0.2-mm sieve. The samples were stored in well-closed vials.

The solid dispersions-coevaporates were prepared in the same ratios by the solvent method in methylene chloride. The solution was poured on glass plates and dried under evaporation. The solid film was crushed and pulverized in a mortar after vacuum-dessication of the sample over P_2O_5 for 12 h, then passed through a 0.2-mm sieve. The samples were stored in well-closed vials.

Optical Microscopy

Optical microscopic observations were carried out on a CH20BIMF binocular microscope, Olympus Optical Co. (Tokyo, Japan).

Scanning Electron Microscopy

Scanning electronic microscopy (SEM) pictures were made with a JSM-5300 (JEOL, Tokyo, Japan). Sample slices were prepared in a liquid nitrogen.

X-Ray Diffractometry

Powder X-ray diffraction (PXRD) patterns were collected in transmission using an X-ray diffractometer (Stoe & Cie GmbH, Darmstadt, Germany) with $Cu-K\alpha_1$ radiation (monochromator: germanium) generated at 8 kW. The powder was packed into the rotating sample holder between two films (PETP). The patterns were analyzed by a position sensitive detector (PSD).

Differential Scanning Calorimetry

Differential Scanning Calorimeter (DSC 7), Perkin Elmer (Norwalk, CT, USA) was used. The heating rate was $10^\circ C/min$ under nitrogen gas flow.

^{13}C NMR/CPMAS

The solid state ^{13}C NMR/cross polarization/Magic-Angle spinning (NMR/CPMAS) measurements were performed with a Bruker AM400 NMR spectrometer (Bruker AXS Inc., Madison, WI, USA) at 4 kHz.

FTIR Spectrometry

A FTIR-8010M spectrometer (Shimadzu, Kyoto, Japan) was used. The samples were prepared as discs in KBr.

Molecular Modeling

The X-ray structures of chiral IBP and NAP were obtained from the Cambridge Structural Database (CSD). The following codes were found: for racemic IBP-IBPRAC and IBPRAC02; for enantiomer IBP: JEKNOC10 and JEKNOC11; for enantiomer NAP: COYRUD and COYRUD11. To ensure the correspondence of the X-ray structures to the substances used in the experiments, the following X-ray structures were used in further analysis: IBP-RAC02 (rac-IBP), JEKNOC10 (S-IBP), and COYRUD11 (S-NAP) (5).

The network of molecules connected by hydrogen bonds (HBs) were generated for each structure using the program Mercury, version 1.2.1 (6). The structures were saved in the mol2 format for a further analysis by the molecular modeling program SYBYL (7). The molecular mechanics methods

implemented in Sybyl, Tripos force field (TFF) and MMFF94, and the semiempirical quantum chemistry method AM1 in MOPAC, version 6 (8) were used for the energy calculations of the structures and for a conformational analysis of the trimer form of PVP. TFF and MMFF94 were applied for optimization with a gradient termination of 0.05 kcal/mol Å using the Powell method and simplex initial optimization. AM1 full optimization of PVP was performed using the key Precise.

RESULTS

Marked differences in the physicochemical properties of the rac-IBP, S-IBP and S-NAP model preparations were established. The results suggested different mechanisms of drug/PVP interaction. Ketoprofen was not included in the current investigation because the glasslike form of its physical mixtures with PVP was of limited physical stability and hence of little practical interest.

Optical Microscopy and SEM Study

The optical microscopic examination of the appearance of the models reveals the following: i) a spontaneous conversion of the crystalline IBP physical mixtures containing approximately 50% PVP and above in a glasslike form after storage at ambient conditions. It is worth to note that S-IBP interacts more strongly with PVP compared to rac-IBP. The spontaneous transformation of the S-IBP/PVP physical mixtures into glasslike state begins during the process of preparation and at relatively low polymer concentration (around 17%). ii) Similarity in the appearance of the IBP physical mixtures and the corresponding solid dispersions. iii) IBP glassy amorphous physical mixtures and solid dispersions remain physically stable over a year. iv) No changes in the initial physical state of all studied NAP physical mixtures and physical instability of the glassy state of the corresponding solid dispersions with high PVP concentrations shortly after their isolation.

The SEM study confirmed the above observations. The SEM photograph of a stored IBP/PVP 1/1.5 (w/w) physical mixture shows no drug crystals (Fig. 1B). Rounded crystals or crystal packs covered by PVP film, however, can be distinguished with a stored 1/0.5 (w/w) sample (Fig. 1A). This picture supports an incomplete interaction due probably to the low PVP content.

Correlation of the X-Ray, DSC, Solid ^{13}C NMR, and FTIR Data

The X-ray powder diffraction, DSC, FTIR, and solid ^{13}C NMR spectroscopy of the studied models showed a strong correlation of the obtained data and a consistency with the optical microscopy and SEM results.

X-Ray Powder Diffraction and DSC

The X-ray and DSC data confirm definitively the amorphous state of the stored IBP physical mixtures (PVP content around and above 50%). For example, the diffractogram of rac-IBP/PVP 1/3 (w/w) physical mixture stored 5 months (Fig. 2) supports the disappearance of the IBP diffraction pattern. It is very similar to those of the corresponding solid dispersion and the pure PVP. The DSC trace (Fig. 3, curve 2) of the same

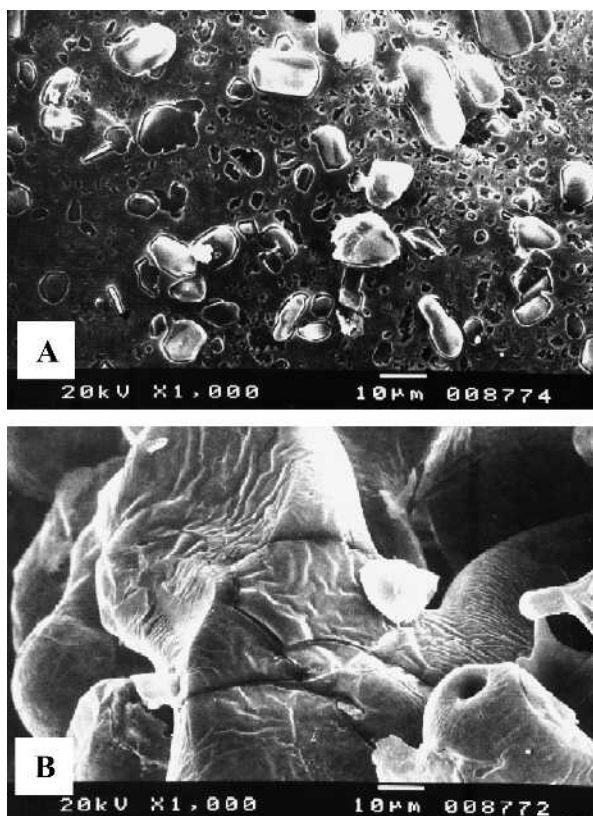


Fig. 1. SEM photographs of stored IPF/PVP physical mixtures: (A) 1/0.5 (w/w); (B) 1/1.5 (w/w).

model, in contrast to that of the freshly prepared sample (Fig. 3, curve 1), does not reveal endothermic or exothermic events and is also typical for amorphous samples (9).

Spectral Study

The ^{13}C NMR spectra of IBP/PVP 1/3 (w/w) physical mixture and the corresponding coevaporate depicted in Fig. 4 illustrate a correlation of the results from NMR spectroscopy with the X-ray and DSC data and confirm the self-transformation of the stored IBP/PVP physical mixtures of polymer content above 50% into solid dispersions.

Comparisons made with published spectra of nontreated IBP and PVP (2) revealed that the spectrum of IBP/PVP 1/3 (w/w) model is not a simple overlay of the spectra of both components. In general, it is more close to the spectrum of PVP. The most important differences appear in the region of the drug aromatic carbons. Unlike the nontreated crystalline IBP, the signals of the physical mixture and the corresponding solid dispersion (Fig. 4) are two, they are significantly broader and of lower intensity probably because of the IBP amorphous state in the drug/PVP sample (10).

The IR spectral investigations have definitively shown differences in the spectral behavior of rac-IBP and S-NAP models. It was established that the most informative changes take place in the regions of the carbonyl-, dimerized hydroxyl groups and in the region of the "fingerprints," respectively.

The IR spectra of nontreated drugs were registered for comparison (Fig. 5, curve 2 and curve 5). Two bands of me-

dium intensity appear at 2633 cm^{-1} and 2731 cm^{-1} in the spectrum of IBP. They can be ascribed to the stretching vibration of the cyclic dimerized hydroxyl groups. These bands are missing in the spectrum of NAP. Other facts in support of the statement that dimeric structures in the crystal packs of NAP do not exist are i) the bending OH absorption band around 1265 cm^{-1} characteristic for free hydroxyl groups and ii) the carbonyl stretching vibrations, which in comparison to those of IBP appear at longer wavelength.

The FTIR spectral analysis of the drug/PVP model preparations reveal that the spectra of all S-NAP/PVP physical mixtures and that of the 1/0.5 solid dispersion (Fig. 5, curve 6) overlay the spectra of the pure NAP and PVP (Fig. 5, curve 5 and curve 1). This fact supports the observation that S-NAP/PVP physical mixtures do not transform spontaneously into solid solutions during storage. The spectrum of the freshly prepared 1/3 solid dispersion (Fig. 5, curve 7) is very similar to that of the PVP. However, the sample is physically very unstable and crystallizes very soon after preparation, fact discussed also in Ref. 11.

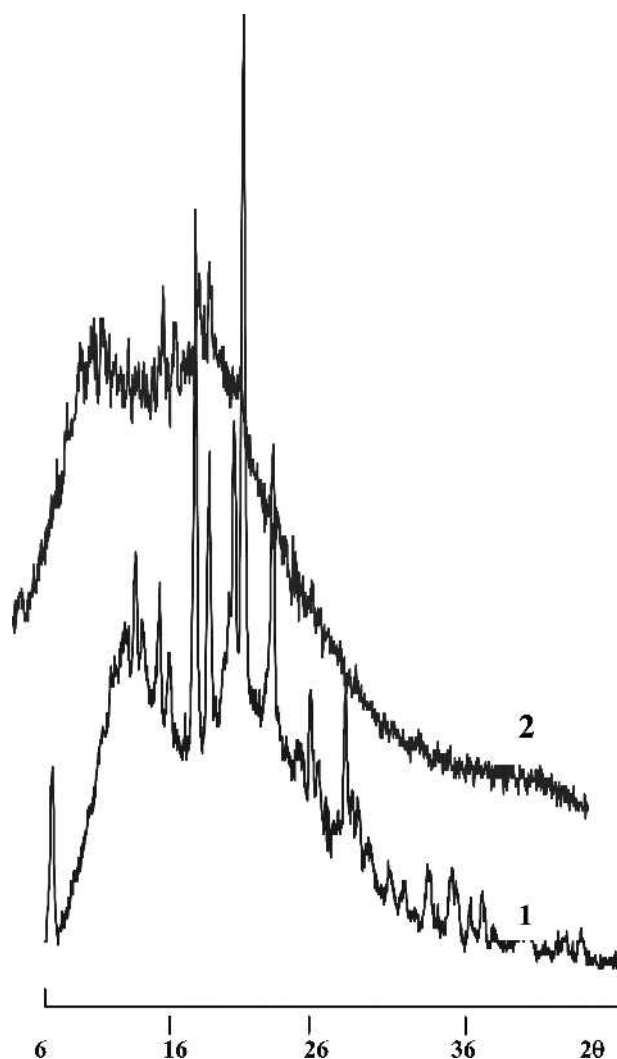


Fig. 2. X-ray diffractograms of IPF/PVP 1/3 (w/w) physical mixtures: 1, freshly prepared; 2, after 5 months storage.

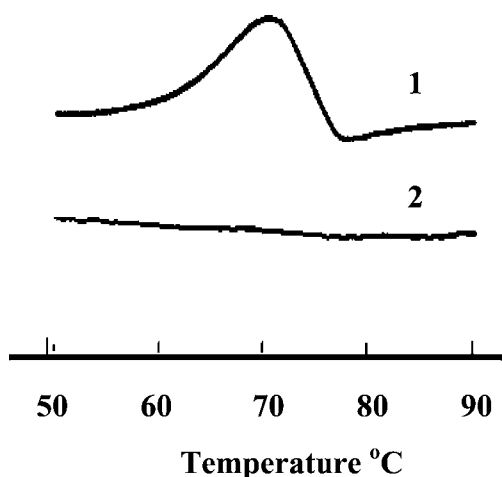


Fig. 3. DSC-traces of IBP/PVP 1/3 physical mixtures: 1, freshly prepared; 2, after 5 months storage.

Unlike, the spectra of the IBP/PVP physical mixtures of glasslike form are similar to those of the corresponding solid dispersions.

In comparison to the spectrum of non-treated IBP the following changes can be observed: i) the vibration peaks intensity at 2633 and 2731 cm^{-1} due to the dimerized OH groups decreases with increase of PVP weight participation (Fig. 5, curve 3 and curve 4). These bands disappear in the spectra of IBP/PVP 1/3 (w/w) models and the bending OH vibrations at 1232 cm^{-1} and the stretching C–O vibrations at 1185 cm^{-1} , respectively, are also missing. ii) Broadening and a bathochromic shift of the band of the carboxylic carbonyl that is most evident with 1/3 model preparations. Absorption interaction with the cyclic amide carbonyl of PVP (around 1760 cm^{-1}) can be also assumed. In support are the reported data by Taylor and Zografis (12) about a similar absorption overlay and spectral changes in the carbonyl region of the IR spectra of amorphous indomethacin/PVP solid dispersions. iii) Marked changes related to out-of-plane bending vibrations of the aryl substituents in the “fingerprint” region, for

example, the disappearance of the very strong peak at 780 cm^{-1} in the spectrum of the 1/3 (w/w) preparations.

The correlation established between the X-ray, DSC, ^{13}C solid-state NMR, and FTIR spectral data suggested differences in the ways of PVP interaction with rac-IBP, S-IBP, and S-NAP. Molecular modeling analysis of the drugs and PVP was further performed to possibly explain the differences observed.

Molecular Modeling Study

The chiral IBP and NAP (Fig. 6) contain similar functional groups and substructures (carboxylic groups and aromatic rings) that can participate in similar type of intermolecular interactions in the crystal (hydrogen bonding, aromatic-aromatic, hydrophobic, steric interactions, etc.). The analysis of the existing crystal packing data of the IBP and NAP structures (5), however, reveals marked differences. The molecules of S-IBP (JEKNOC10) and rac-IBP (IBP-RAC02) are arranged in the crystal lattices as dimers in which the carboxylic groups of two neighbor molecules form HBs between each other: the cyclic dimer of S-IBP is formed from two molecules of one and the same S-configuration but of different conformational states, and the dimer of rac-IBP is formed by one R- and one S-molecules (13,14). S-NAP (COYRUD11) has a catemer arrangement in which one molecule interacts by hydrogen bonding with two neighbor molecules thus forming helicoids parallel to a screw axis of 2nd order (15).

To get a deeper insight into the differences of the crystal arrangement and their possible impact on the interaction of the drugs with PVP a comparative analysis of the drugs crystal structures and of the intermolecular interactions in the crystals is further described.

Analysis of the HB Characteristics

Table I represents the HB angles and lengths measured. Despite the differences observed, all angles and lengths are close to the typical values for HB (16) (see the legend to Table I). The angle O–H...O = in the catemer S-NAP has the high-

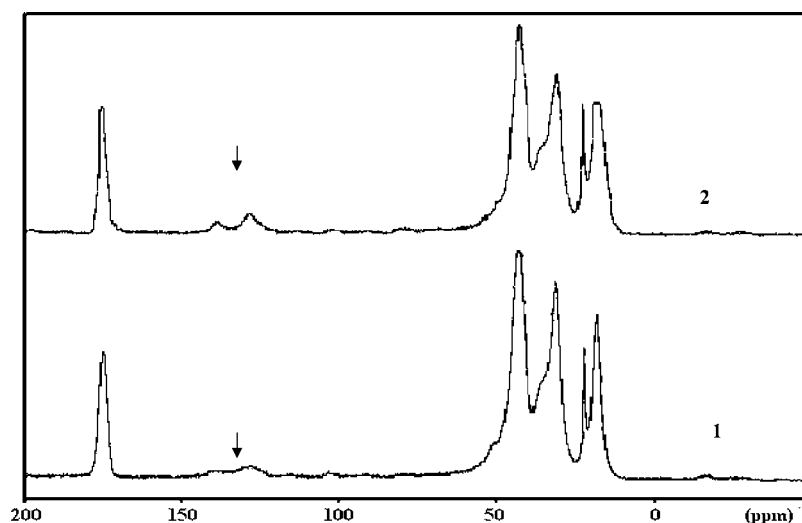


Fig. 4. ^{13}C NMR/CPMAS spectra of IPF/PVP 1/3 (w/w): 1, physical mixture; 2, solid dispersion.

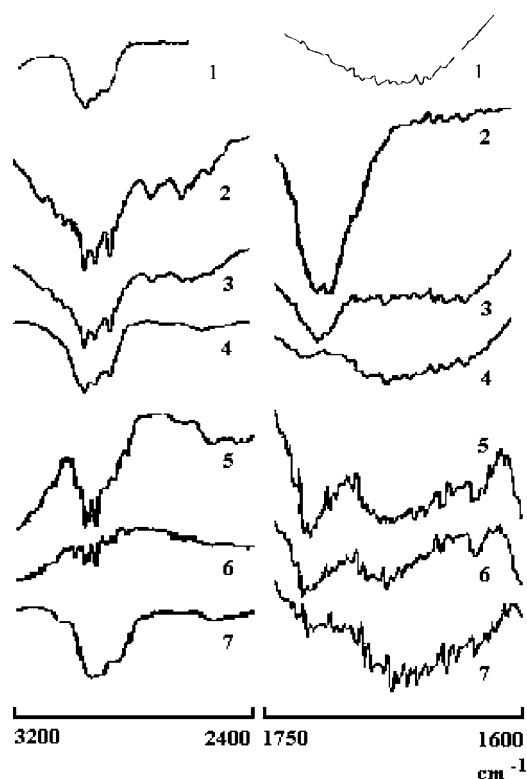


Fig. 5. FTIR spectra in the regions 3200 cm^{-1} to 2400 cm^{-1} and 1750 cm^{-1} to 1600 cm^{-1} of 1, PVP; 2, IPF; 3, IPF/PVP 1/0.5 (w/w) SD; 4, IPF/PVP 1/3 (w/w) SD; 5, NAP; 6, NAP/PVP 1/0.5 (w/w) SD; 7, NAP/PVP 1/3 (w/w) SD.

est value and the HBs lengths are the longest and closest to the optimal length of 2.7 \AA . Unlike, the HB angles and lengths of S-IBP are the lowest and deviate mostly from the optimal values suggesting that HBs of S-IBP dimers are mostly tensed by the crystal packing forces.

Further, it is worth noting that the HB angles and lengths in rac-IBP as well as in S-NAP are fully identical. In contrast, the angles $\text{O-H}\cdots\text{O}=\text{}$ of the two HBs in the cyclic dimer of S-IBP differ by about 7° and small differences are also observed for the HB lengths (Table I). As already reported (13,14,17), the dimer of rac-IBP is formed by two hydrogen bonds of one and the same geometry over the crystallographic center of inversion (space group $P2_1/c$). The unit cell of S-IBP is asymmetric (space group $P2_1$), which provokes nonequivalence of the geometry of both HBs.

The above analysis of the HB characteristics suggests that the asymmetric and tensed HBs in the dimer of S-IBP might be more easily destabilized compared to the other structures studied providing external HB acceptor groups (e.g., the amide oxygens of PVP) compete for hydrogen bonding with the dimer COOH donor groups.

Analysis of the Aromatic-Aromatic Interactions

All structures possess aromatic rings that suggest the possibility for intermolecular aromatic-aromatic interactions in the crystals. S-NAP compared to IBP possesses a naphthalene ring that, probably, set the catemer pattern of its crystal arrangement (see "Discussion"). The presence of a two-ring fused aromatic system suggests stronger intermolecular aro-

matic-aromatic interactions in the crystal of NAP. To get an approximate presentation about the character of the aromatic-aromatic interactions, we have analyzed the orientations of the aromatic rings in the crystal structures of S-IBP and S-NAP. The findings of Hunter *et al.* (18) who determined the distances (the offset between the centroids of the rings) and the angle regions (the interplanar angles) for favorable and unfavorable aromatic-aromatic interactions were used as a basis. The angles between the ring planes and the offsets between the centroids of the closest aromatic rings were measured. The results are shown in Fig. 7A and Fig. 7B, respectively. As seen from the figures in both crystals, independently of the motif (dimer or catemer), the face-to-face offset stacked and edge-to-face orientations take place, however, they differ in the values of the interplanar angles and offsets. The offset between the closest rings for S-NAP ($\sim 5\text{ \AA}$) is shorter than that for S-IBP ($\sim 6.8\text{ \AA}$) and falls into the middle of the interval of the favorable face-to-face stacked offset interactions (approximately between 3.2 \AA and 7.2 \AA) (19). In case of the edge-to-face orientation, again the offsets between the closest aromatic rings are shorter for S-NAP ($\sim 1\text{ \AA}$) than for S-IBP ($\sim 3\text{ \AA}$) and the interplanar angles differ by about 15° , both being in the intervals of the values of favorable interactions.

The above analysis points to S-NAP as a drug that is well stabilized by aromatic-aromatic interactions. In support of similar conclusions are also the results of Perlovich *et al.* (15) who have studied the contribution of different energetic terms of the structural fragments of NAP molecule. The biggest impact (43.2%) was attributed to the naphthalene-naphthalene interaction.

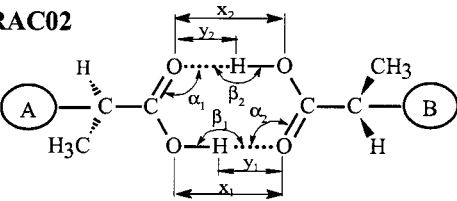
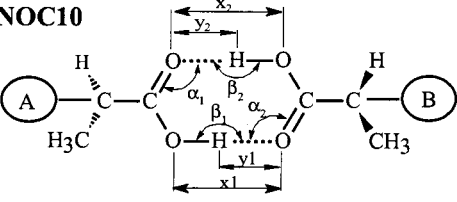
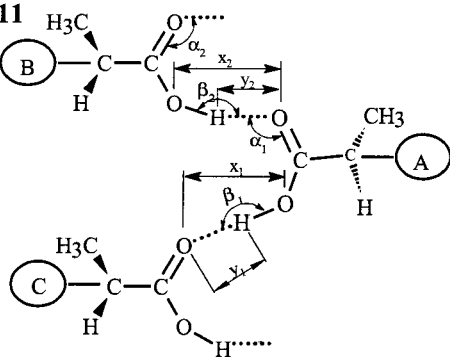
Analysis of the Molecular Energies in the IBP Dimers


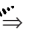
To further check how stable are the dimers in different crystal arrangements of IBP, they were analyzed by molecular mechanics. First, the whole dimers were studied and second, the carboxylic groups only were considered. Table II summarizes the results of the energy calculations by TFF and MMFF94. The energies were calculated with Gasteiger-Huckel charges in TFF and with MMFF94 charges in MMFF94.

As seen from Table II, the energies of the dimers calculated with the same force field differ between. The rac-IBP has the lowest E_{TOT} in both fields and the same holds also for its COOH- groups. Analysis of the terms that contribute mostly to E_{TOT} shows that the highest energy value of the COOH-dimer in S-IBP is related to the bond-stretching energy E_{BS} , van der Waals E_{VDW} , and electrostatic (1-4) E_{ELE}^{1-4} interactions. By TFF these terms represent about 53% (E_{BS}), 29% (E_{VDW}), and 7% (E_{ELE}^{1-4}) of E_{TOT} . In MMFF94, the highest contribution to E_{TOT} have again E_{BS} (34%) and E_{ELE}^{1-4} (39%). It is worth noting that E_{BS} is comparable in both, the whole dimer structure and the COOH-group for S-IBP (Table II) in both force fields, suggesting that the COOH groups in the S-IBP dimers are much more tensed by crystal packing forces than those in rac-IBP. This result confirms once again the suggestion made above on the basis of the HB characteristics for the internally tensed HB complex in S-IBP.

Further, the single molecules in the IBP dimers were compared in relation to their conformations and energies. First, the geometry of S-conformation of rac-IBP was com-

Table I. Geometrical Characteristics (Angles and Lengths) of the Hydrogen Bonds in the Crystal Structures of the Studied Drugs (The Structures of COOH Groups Are Only Shown for Simplicity)

Refcode	Structure ^a	HB Characteristics ^b	
		Angles (°)	Distances (Å)
IBPRAC02		$C=O\cdots H$ $\alpha_1 = 125.30$ $\alpha_2 = 125.30$ $OH\cdots O=$ $\beta_1 = 174.60$ $\beta_2 = 174.60$	$O(H)\cdots O=$ $x_1 = 2.657$ $x_2 = 2.657$ $(O)H\cdots O=$ $y_1 = 1.624$ $y_2 = 1.624$
JEKNOC10		$C=O\cdots H$ $\alpha_1 = 115.96$ $\alpha_2 = 115.78$ $OH\cdots O=$ $\beta_1 = 153.03$ $\beta_2 = 160.20$	$O(H)\cdots O=$ $x_1 = 2.629$ $x_2 = 2.655$ $(O)H\cdots O=$ $y_1 = 1.466$ $y_2 = 1.405$
COYRUD11		$C=O\cdots H$ $\alpha_1 = 154.00$ $\alpha_2 = 154.00$ $O(H)\cdots O=$ $\beta_1 = 173.20$ $\beta_2 = 173.20$	$O(H)\cdots O=$ $x_1 = 2.681$ $x_2 = 2.681$ $(O)H\cdots O=$ $y_1 = 1.922$ $y_2 = 1.922$

^a A, B, C: molecule residues. Stereo bonds:  \Rightarrow facing away from the viewer;  \Rightarrow facing toward the viewer.

^b Typical values of HB characteristics: angle $C=O\cdots H \Rightarrow 100 + 180^\circ$; angle $O(H)\cdots O= \Rightarrow >150^\circ$; distance $O(H)\cdots O= \Rightarrow 2.7 \text{ \AA}$; distance $(O)H\cdots O= \Rightarrow 1.8 \text{ \AA}$.

pared to any of the two S-conformations in the dimer of S-IBP. Although the orientation of the COOH-group in one of the S-form in S-IBP corresponded closely to that of the S-form in rac-IBP, in the other S-form the carbonyl oxygen and the hydroxyl group had an opposite orientation. This orientation is to be expected considering that the same type enantiomers form the dimer of S-IBP, and thus different conformations of the same enantiomer form the dimer structure of S-IBP in agreement with Refs. 13,14,17. Correspondingly, the energy calculations show different values for the single enantiomers in S-IBP. The results of the energy calculations by TFF and MMF94 are summarized in Table III. As seen from the table, the single molecules in S-IBP have different energies, while the same energies are recorded for the S- and R-forms in the rac-IBP. Additionally, the energy values of the S- and R-structures in the racemate calculated by both methods are significantly lower compared to the enantiomers of S-IBP. These results point to the fact that the dimers formed by the enantiomers of different types are more stable com-

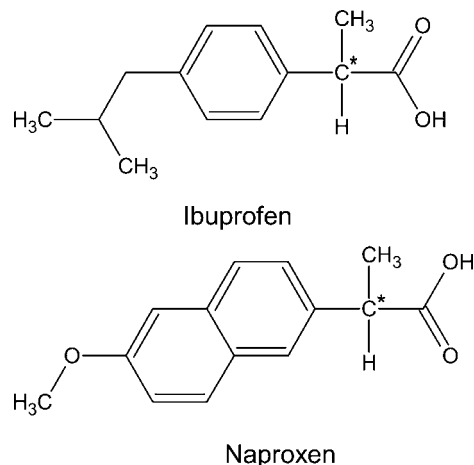


Fig. 6. Chemical structures of ibuprofen and naproxen; C* is the chiral atom.

Table II. Energies of IBP Structures Calculated by Molecular Mechanics

Energies ^a (kcal/mol)	Whole dimer		COOH groups		Whole dimer		COOH groups	
	rac-IBP (IBPRAC02)		rac-IBP (IBPRAC02)		S-IBP ^b (JEKNOC10)		S-IBP (JEKNOC10)	
	TFF	MMFF94	TFF	MMFF94	TFF	MMFF94	TFF	MMFF94
E _{BS}	11.488	11.237	0.583	2.604	119.174	65.450	100.078	54.657
E _{AB}	4.883	8.944	0.348	0.176	7.765	16.680	2.004	4.822
E _{TOR}	4.006	-0.173	0.038	3.246	3.920	-0.150	0.064	3.273
E _{OOB}	0.739	0.087	0.000	0.000	1.406	0.183	0.000	0.000
E _{SB}	—	-0.358	—	0.259	—	-0.636	—	-0.246
E _{VDW} ¹⁻⁴	9.824	59.991	2.137	-0.032	16.563	65.269	5.235	0.000
E _{VDW}	-0.886	5.446	2.174	4.990	55.930	16.678	54.845	13.863
E _{ELE} ¹⁻⁴	-12.679	-46.886	-11.658	-60.241	-14.335	-51.234	-13.082	-63.722
E _{ELE}	-8.783	13.785	-9.589	-19.651	-12.736	12.182	-13.372	-21.207
E _{TOT}	8.592	52.073	-15.967	-68.649	177.687	124.422	135.412	-8.559

^a E_{BS}, bond stretching energy; E_{AB}, angle bending energy; E_{TOR}, torsional energy; E_{OOB}, out-of-plane bending energy; E_{SB}, stretch-bend energy; E_{VDW}¹⁻⁴, 1-4 van der Waals energy; E_{VDW}, van der Waals energy; E_{ELE}¹⁻⁴, 1-4 electrostatic energy; E_{ELE}, electrostatic energy; E_{TOT}, total energy.

^b An arbitrary selected dimer.

pared to those of the dimers formed by the same type enantiomers.

Analysis of the Distances and Angles

Although of the same dimer type, the crystal structures of rac-IBP and S-IBP differ by the distances between the same functional groups and also by the angles between the planes of the COOH-dimers. The distances between the O = atoms of the COOH groups in the crystal structures are shown in Fig. 8A for rac-IBP and Fig. 8B for S-IBP. These distances were intentionally chosen in order to be related to the distances between the amide oxygens in the PVP structure (see below) that, presumably, could compete with these atoms for hydrogen bonding with the H-atoms of the hydroxyl groups. The distance between the oxygen atoms of the neighbor dimers is 5.561 Å in rac-IBP and 5.764 Å in S-IBP.

The planes formed by the atoms of the COOH-groups were built and the angles between the planes of two neighbor dimers were also measured. The angle between the planes of the dimers 1 and 2 was ~135° in rac-IBP (Fig. 7A) and ~130° in S-IBP (Fig. 8). Additionally, as seen from the figures, in S-IBP the dimers of the same orientation are apart each other (14.400 Å), while they are closer located in the racemate (10.506 Å).

The translational period of the catemer structure in S-NAP is 5.793 Å (Fig. 8C), which falls between the two limit values of 6.5 Å and 5 Å for catemer motives of monofunctional carboxylic acids reported in Ref. 19.

Table III. Energies of the Single Structures in the IBP Dimers

Dimer	E _{TFF} (kcal/mol)	E _{MMFF94} (kcal/mol)
rac-IBP (IBPRAC02)		
S	8.506	33.916
R	8.506	33.916
S-IBP (JEKNOC10)		
S1	78.486	71.831
S2	58.860	61.632

The above analyses of the crystal structures of the drugs studied show that there are essential differences in the way the structures are arranged in the crystal. All these differences suggest their impact on the drug behavior in a solid

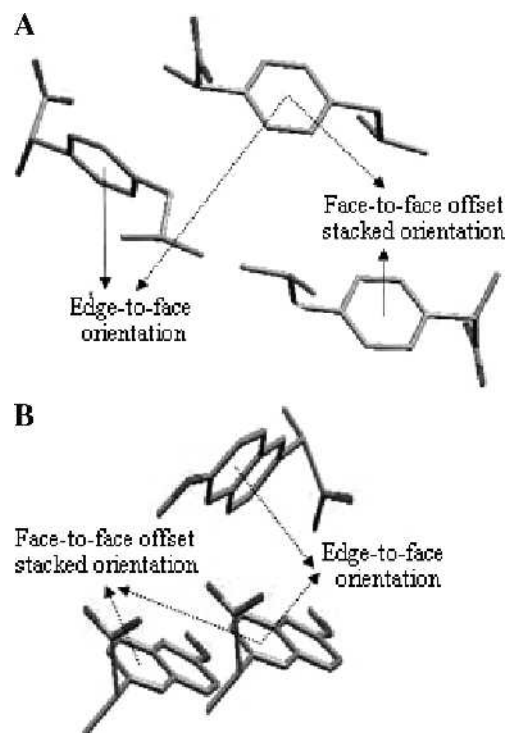


Fig. 7. Aromatic-aromatic interactions in the crystal structures: C-atoms are shown in gray, O-atoms are shown in dark gray, H-atoms are not shown. (A) S-IBP (refcode JEKNOC10). Face-to face orientation: plane angle ~0°, offsets between the centroids of the closest rings ~6.8 Å; edge-to-face orientation: plane angle ~70°, offsets between the centroids of the closest rings ~3 Å. (B) S-NAP (refcode COYRUD11). Face-to face orientation: plane angle ~0°, offsets between the centroids of the closest rings ~5.0 Å; edge-to-face orientation: plane angle ~55°, offsets between the centroids of the closest rings ~1 Å.

state in presence of PVP. To get a deeper insight into the possible ways of interactions, we modeled also the structure of PVP.

Molecular Modeling Analysis of Polyvinylpyrrolidone

The trimer structure of PVP was built using the fragmental library in SYBYL. Each fragment was optimized by MMFF94, the fragments were joined and the resulting monomer was also optimized. The trimer was built by joining three monomers and the final structure was optimized once more by MMFF94 and AM1 using the key Precise. The so-derived structure was subjected to a systematic conformational search with 7 rotatable bonds (RBs) (assigned as 1, 2, 3, 4, 5, 6, and 7 in Fig. 9A) with 30° increment and the default bump check (0.95 for general van der Waals interactions, 0.87 for 1-4 interactions, and 0.65 for H-bond interactions) using MMFF94. In the energy interval from -46.117 to -14.63 kcal/mol, 2697 conformations were generated. Taking into account that at room temperature, conformations up to about 3 kcal above the global energy minimum are significantly populated and also the possible errors due to the systematic search, the energy interval of 5 kcal/mol was set in the conformations sorted by the energy values and 40 were finally selected in the lowest energy interval from -46.117 to -41.123 kcal. All these conformations were additionally minimized by MMFF94 and AM1, and the distances between the amide oxygens of the three monomers were recorded. Analysis of the resulted geometries revealed that the energetically most favorable conformations (those with the lowest heats of formation (HF) \approx -127 kcal, as calculated by AM1 after the full energy optimization using the key Precise) were those in which the O= atoms in the end monomers (assigned by 1 and 3 in the figure) faced the same direction and the O= atom in the intermediate monomer (assigned by 2) was directed at about 125° toward the end monomers (Fig. 9B). In this orientation the distances between the O= atoms were almost equal, in average 5.8 Å (they ranged from 5.76 Å to 5.83 Å among the first 10 conformers with the lowest HF).

The AM1 charges of the O= atoms were also similar and fell into the range of -0.360 to -0.380 e. The Gasteiger-Huckel partial atomic charges were also assigned and compared to those of the drugs studied. Preferences were given to the topological charges, because they were conformationally independent. As the trimer and not the polymer form of PVP (as it appears in reality) was only considered, the topological charges appeared to be the more appropriate than the quantum-chemical ones for comparison to the drug charges. The amide oxygen atom in PVP had the Gasteiger-Huckel charge of -0.397 e. For comparison, the same type atomic charge of the O= in the carboxylic group of rac-IBP, S-IBP, and S-NAP was -0.367 e. Thus, the charges of the carboxylic O= atom in the drug structures and of the amide =O atom in the PVP trimer have close values.

DISCUSSION

On the basis of the above results, the following hypothesis can be proposed.

The differences in the interactions of rac-IBP, S-IBP, and S-NAP with PVP in a solid state can be related to the way the molecules are arranged in the crystal and the differences in

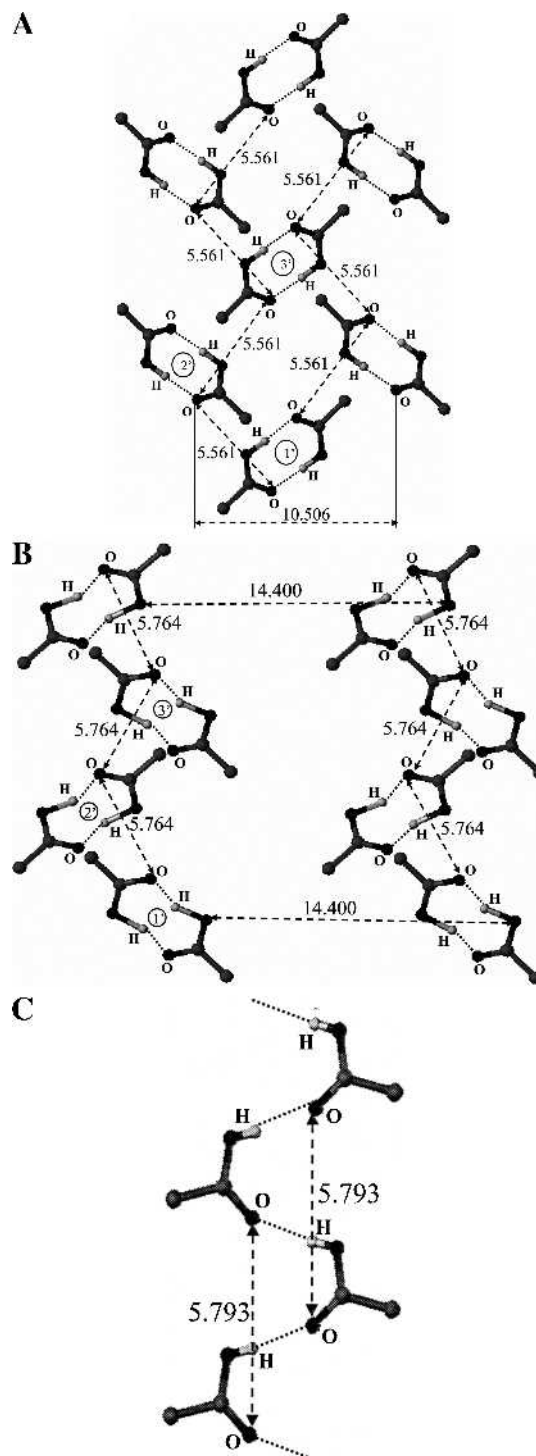


Fig. 8. Distances and orientations of the COOH-groups in the network of molecules connected by HBs in the crystal structures. (A) rac-IBP (refcode IBRAC02), (B) S-IBP (refcode JEKNO10), (C) S-NAP (refcode COYRUD11). C-atoms are shown in gray, O-atoms are in dark gray, and H-atoms are in light gray (for clarity, the H-atoms in the OH-groups are only shown); dotted lines represent hydrogen bond (HB) interactions between the COOH-groups; the angles between the COOH-planes of two neighbor dimers 1' and 2' are $\sim 135^\circ$ in rac-IBP and $\sim 130^\circ$ in S-IBP.

the intermolecular interactions. In case of rac-IBP and S-IBP, the dimer organization takes place, while the crystal of S-NAP has the catemer arrangement. As suggested in the case study of 2-phenoxypropionic acid (19), whether a dimer or a catemer motif is formed appears to depend on the nature of the substituent at the COOH group. Indeed, in case of S-NAP, the presence of the naphthalene ring in the α -position may give the preference to catemer organization due to the stronger aromatic-aromatic interactions compared to the IBP benzene-benzene intermolecular interactions. In relation to the purpose of this study, the more essential appears the fact that the catemer arrangement of S-NAP seems to be well stabilized by HB and aromatic-aromatic interactions as demonstrated by the HB characteristics, aromatic interplanar angles, and offsets. Additionally, in the S-NAP catemer, each molecule interacts by hydrogen bonding with two more molecules, thus having two more molecules involved simultaneously in the same HBs; in the IBP dimer, one molecule makes hydrogen bonding with one more molecule, thus having two molecules involved in the same HBs. Further, the dimer arrangement of rac-IBP appears to be more stable compared to S-IBP, which crystal structure is more tensed by the crystal packing forces as evident from the HB-complex asymmetry and molecular energies (Tables I, II, and III). Additionally, compared to rac-IBP, the dimer arrangement of S-IBP is characterized by larger distances between the parallel dimers (Fig. 8A and Fig. 8B). As noticed by Romero and Rhodes (20), there are more exposed carboxyl groups and less hydrophobic layers on the crystal surface of S-IBP compared to rac-IBP suggesting still easier possibility for destabilization of the S-IBP crystal ordering. Thus, it can be expected that any external competition for hydrogen bonding (presumably the amide oxygens of PVP) would give preferences to a more relaxed conformation of the S-IBP dimer.

In all structures, the distances between the O= atoms (5.561 Å, 5.764 Å, and 5.793 Å for rac-IBP, S-IBP, and S-NAP, respectively) are similar and close to those of the lowest energy conformers of PVP (~5.8 Å, Fig. 9). Indeed, the distance between the O= atoms in S-IBP is closest to those of PVP, however, small deviations between the atoms are likely to take place. Also, the topological atomic partial charges of the amide O= atoms of PVP (-0.397 e) are comparable (even slightly higher) to those of the O= atoms in the -COOH group of the drugs (-0.367 e), suggesting the possibility for the amide O= atom to compete with the carboxylic =O atom for HB-interaction with the H-atom of the hydroxyl groups. The AM1 charges also suggest such possibility, although, as mentioned above, this comparison is not fully correct in relation to conformation-dependent atomic charges. Nevertheless, according to the distances and charges, all structures are likely to perform HB-interactions with PVP. In case of rac-IBP and S-IBP, the mutual orientation of the dimer complexes (at about 135° and 130°, respectively) corresponds approximately to the angle between the amide oxygens in PVP (about 125°). As shown schematically in Fig. 10A and 10B for rac-IBP and S-IBP, respectively, the arrangement of the IBP dimers favors the simultaneous interactions of each monomer unit of PVP (assigned by 1, 2, 3, etc.) with each dimer of IBP (assigned correspondingly by 1', 2', and 3'). In contrast, in S-NAP, two of every three monomer units of PVP face the catemer carboxylic groups (Fig. 10C). It can be presumed that the interaction of PVP (by 2 out of 3 monomer

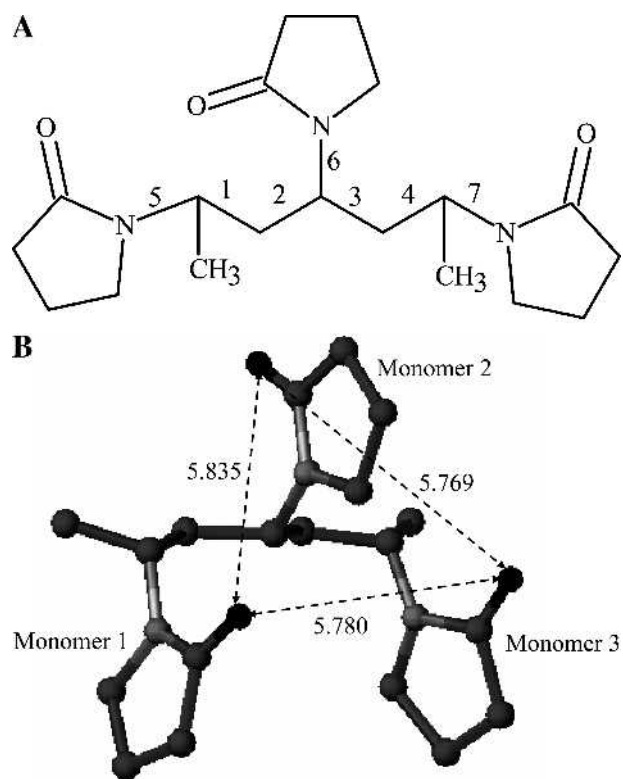


Fig. 9. Structural formula of the PVP trimer with the rotatable bonds 1, 2, 3, 4, 5, 6, and 7 (A) and the 3D structure of the lowest energy conformer of the PVP trimer with distances and angles between the amide oxygens (B). C- and N-atoms are shown in gray, O-atoms are shown in dark gray; H-atoms are omitted; each monomer in the PVP trimer is assigned a number from 1 to 3.

units) with S-NAP stabilized by intermolecular interactions is energetically unfavorable. In contrast, S-IBP and rac-IBP dimers are likely to have energetically favorable interactions with the PVP monomer units. It is reasonable to suggest that the PVP chains may influence the arrangement of the dimer crystal structures of rac-IBP and S-IBP in a way that destroys the HBs but keeps the initial order of the IBP molecules allowing simultaneously some relaxation of the crystal structures. Considering the asymmetry and the high internal tension of the crystal structure of S-IBP compared to rac-IBP, this influence could be expected to be stronger for S-IBP than for rac-IBP. This agrees with the thermochemical characteristics of rac-IBP and S-IBP (14) that suggest higher reactivity of S-IBP. Such an arrangement of the IBP and PVP molecules can be considered as an intermediate state between the stable crystal and amorphous forms of the drug. Our experimental results on the interactions of rac-IBP and S-IBP with PVP agree with this hypothesis.

CONCLUSIONS

The differences in the interaction of PVP with rac-IBP, S-IBP, and S-NAP can be related to the differences in their crystal structures. The catemer arrangement and the intermolecular interactions in the crystal of S-NAP do not presume favorable HB-interactions with the PVP chains. In contrast, the dimer organized rac-IBP and S-IBP are likely to perform favorable aromatic as well as HB interactions with the amide oxygens of PVP monomer units. The correlation between the

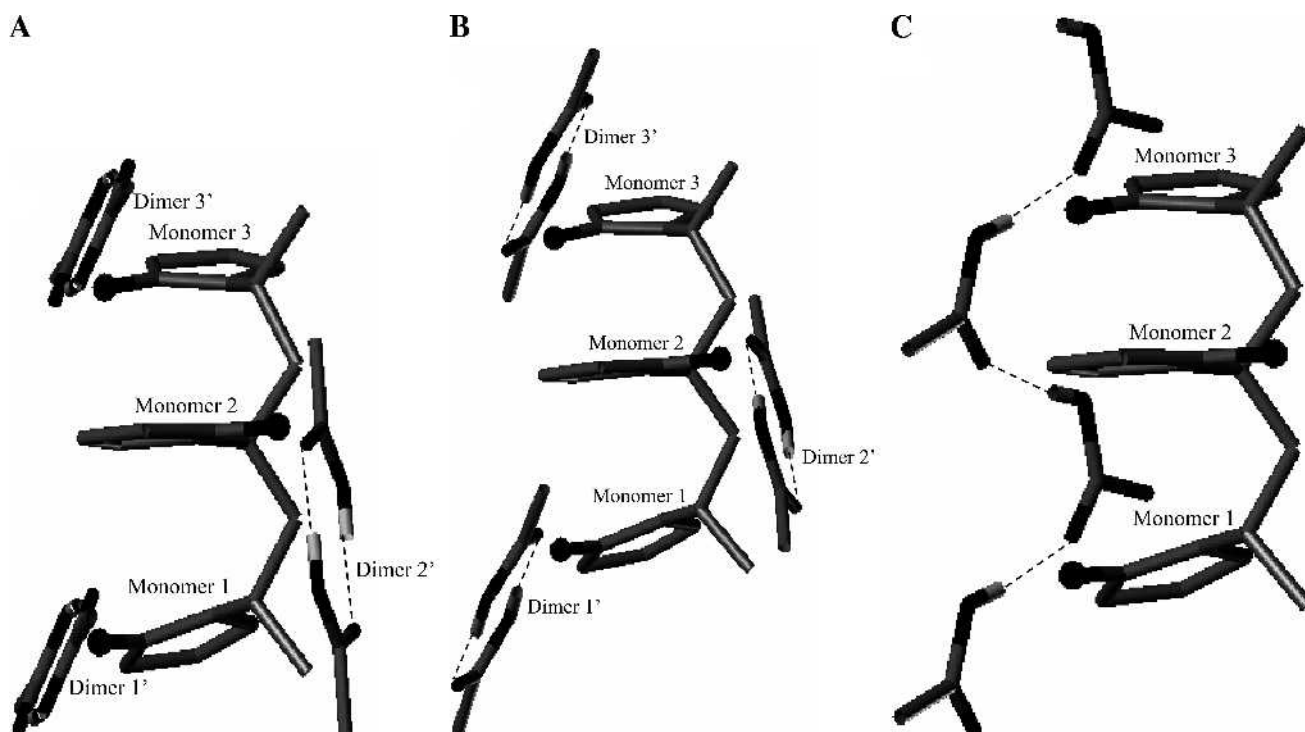


Fig. 10. Schematic presentation of the putative orientation of the PVP-trimer toward the COOH-groups in the crystal structures of (A) rac-IBP (refcode IBRAC02), (B) S-IBP (refcode JEKNOC10), (C) S-NAP (refcode COYRUD11).

experimental and molecular modeling results confirms this assumption.

ACKNOWLEDGMENTS

We would like to thank Alexander von Humboldt Foundation for the fellowship granted to one of the authors and Dr. Norbert Rasenack (Department of Pharmaceutics and Biopharmaceutics, Christian-Albrecht-University, Kiel, Germany) for performance of the X-ray analysis.

REFERENCES

1. H. Sekizaki, K. Danjo, H. Eguchi, Y. Yonezawa, H. Sunada, and A. Otsuka. Solid state interaction of ibuprofen with polyvinylpyrrolidone. *Chem. Pharm. Bull. (Tokyo)* **43**:988–992 (1995).
2. C. Hops. 2000. Änderung der physico-chemischen Eigenschaften von Arzneistoffen durch Modifikation von Habitus und Kristallstruktur. Ph.D. Thesis, Kiel, 2000.
3. A. Romero, L. Savastano, and C. Rhodes. Monitoring crystal modifications in systems containing ibuprofen. *Int. J. Pharm.* **99**: 125–134 (1993).
4. P. Nikolova and S. Bogdanova. Poly(vinylpyrrolidone)/propionic acid derivatives interactions – comparative FT-IR study. Proceedings of Xith Panhellenic Pharmaceutical Congress, March, 2003, Athens, Greece.
5. Cambridge Crystallographic Data Centre, Cambridge, UK.
6. Mercury 1.2.1. CCDC 2001–2004. Available at <http://www.ccdc.cam.ac.uk/mercury/>.
7. SYBYL, version 6.8, Tripos Inc., St. Louis, MO.
8. QCPE, Department of Chemistry, Indiana University, Bloomington, IN.
9. A. Burger, K. Toller, and W. Schiermeier. RS-ibuprofen and S-ibuprofen (Dexibuprofen) – binary system and unusual solubility behaviour. *Eur. J. Pharm. Biopharm.* **43**:142–147 (1996).
10. P. Saindon, N. Cauchon, P. Sutton, C.-J. Chang, G. Peck, and S. Byrn. Solid state nuclear magnetic resonance (NMR) spectra of pharmaceutical dosage forms. *Pharm. Res.* **10**:197–203 (1993).
11. G. Bettinetti and P. Mura. Dissolution properties of naproxen in combinations with polyvinylpyrrolidone. *Drug Dev. Ind. Pharm.* **20**:1353–1366 (1994).
12. L. Taylor and G. Zografi. Spectroscopic characterization of interactions between PVP and indomethacin in amorphous molecular dispersions. *Pharm. Res.* **14**:1691–1698 (1997).
13. A. Freer. Structure of (S)-(+)-. *Ibuprofen. Acta Cryst.* **49C**:1378–1380 (1993).
14. G. Perlovich, S. Kurkov, L. Hansen, and A. Bauer-Brandl. Thermodynamics of sublimation, crystal lattice energies, and crystal structures of racemates and enantiomers: (+)- and (±)-ibuprofen. *J. Pharm. Sci.* **93**:654–666 (2004).
15. G. Perlovich, S. Kurkov, A. Kinchin, and A. Bauer-Brandl. Thermodynamic of solutions III: comparison of the solvation of (+)-naproxen with other NSAIDs. *Eur. J. Pharm. Biopharm.* **57**:411–420 (2004).
16. H.-J. Boehm, G. Klebe, and H. Kubinyi. *Wirkstoffdesign*, Spectrum Akad. Verl.Hedelberg, 1996.
17. N. Shankland, A. Florence, Ph. Cox, Ch. Wilson, and K. Shankland. Conformational analysis of Ibuprofen by crystallographic database searching and potential energy calculation. *Int. J. Pharm.* **165**:107–116 (1998).
18. C.A. Hunter, J. Singh, and J.M. Thornton. Pi-pi interactions: the geometry and energetics of phenylalanine-phenylalanine interactions. *J. Mol. Biol.* **218**:837–846 (1991).
19. H. O. Sorensen and S. Larsen. Hydrogen bonding in enantiomeric versus racemic mono-carboxylic acids; a case study of 2-phenoxypropionic acid. *Acta Crystallogr. B* **59**:132–140 (2003).
20. A. Romero and C. Rhodes. Stereochemical aspects of the molecular pharmaceutics of ibuprofen. *J. Pharm. Pharmacol.* **45**: 258–262 (1993).